Mapping the Thermal Lithosphere and Melting across the Continental US

Ryan Porter[1]; Mary Reid[1]

[1]Northern Arizona University

ABSTRACT

The thermal regime of continental lithosphere plays a fundamental role in controlling the behavior of tectonic plates. In this work, we assess the thermal state of the North American upper mantle by combining shear-wave velocity models calculated using data from the EarthScope facility with empirically derived anelasticity models and basalt thermobarometry. We estimate the depth to the thermal lithosphere-asthenosphere boundary (LAB), defined as the intersection of a geotherm with the 1300° C adiabat. Results show lithospheric thicknesses across the contiguous US vary between ~40 km and > 200 km. The thinnest thermal lithosphere is observed in the tectonically active western US and the thickest lithosphere in the mid-continent. By combining geotherm estimates with solidus curves for peridotite, we show that a pervasive partial melt zone is common within the western US upper mantle and that partial melt is absent in the eastern and central US without significant metasomatism.

PLAIN LANGUAGE SUMMARY

The lithosphere, which is the upper most mechanical layer of the earth, makes up tectonic plates and can vary in thickness laterally. Thickness variations influence the location of volcanoes and where deformation occurs when forces act on the lithosphere. Lithospheric thicknesses can be estimated by examining the thermal properties of the uppermost mantle. We

integrate seismic observations and lab results to calculate temperatures for the upper mantle in the continental US and compare these to geochemical proxies for temperature. We then use these temperature results to estimate lithospheric thickness and map where melt is predicted within the upper mantle. Results show thin lithosphere and the presence of melt in the western US. Thicker lithosphere and an absence of melt are observed in the central and eastern US.

INTRODUCTION

The lithosphere-asthenosphere boundary (LAB) is a fundamental rheological boundary in the earth, separating the rigid lithosphere, which makes up the earth's tectonic plates, from ductile asthenosphere below. The decrease in seismic velocity with respect to depth often observed at this boundary is attributed to changes in rheology due to increased temperatures at depth, the presence of melt, and/or the transition from a chemically depleted mantle lithosphere to a more enriched asthenosphere [e.g. *Jordan*, 1975; *Fischer et al.*, 2010; *Yuan and Romanowicz*, 2010]. Understanding the thermal state of the upper mantle is important for better understanding of the nature of the LAB in regions of both active tectonism and tectonic quiescence, and the behavior of lithosphere in general. To better understand the physical state of the mantle beneath North America, we utilize experimentally derived anelasticity data to convert shear velocities calculated using data from the EarthScope Transportable Array to temperatures and compare these results with basalt equilibration pressures and temperatures based on thermobarometry. We then present a new three-dimensional temperature model for the uppermost mantle beneath the continental US, which allows for a better understanding of upper-mantle rheology and the nature of the LAB across the continent.

METHODOLOGY

Shear Velocities

To calculate upper-mantle temperatures, we utilize a shear velocity model where velocities were calculated by inverting ambient noise and wave gradiometry data at periods between 8 and 150 seconds [*Liu and Holt*, 2015; *Porter et al.*, 2016]. We use a linearized least squares inverse method where all phase velocity measurements are weighted equally to invert from phase velocity to shear velocity [*Herrmann and Ammon*, 2002]. The use of phase velocity measurements out to a period of 150 seconds allows for the calculation of a shear velocity model that extends down to ~200 km depth, which is deeper than many other existing surface wave measurements for the region allow for. In the shear velocity inversion, crustal and basin thicknesses are constrained using data from the Earthscope Automatic Receiver function Survey (EARS) [*Crotwell and Owens*, 2005], and the Laske and Masters [1997] global sediment thickness map.

Seismic Temperature Calculations

We use seismic velocities and pressure estimates to calculate temperatures for the upper mantle across the continental US. Within the mantle, the dominant control on seismic velocity is thought to be temperature, with the roles of factors such as composition, melt, and grain size debated and less constrained. Experimentally derived data from Isaak [1992] are used to calculate the effects of temperatures on the unrelaxed shear modulus for olivine. At high temperatures (>~900° C) anelastic effects are pronounced and a linear relationship between increased temperature and anharmonic decreases in elastic moduli no longer holds [*Goes et al.*, 2000; *Cammarano et al.*, 2003; *Faul and Jackson*, 2005; *Priestley and Mckenzie*, 2006; *Jackson et al.*, 2008; *Jackson and Faul*, 2010; *McCarthy et al.*, 2011; *Priestley and Mckenzie*, 2013]. To

account for this, data from McCarthy et al. [2011] are used to relate velocities to temperature. Using these anharmonic and anelastic velocity/temperature relationships, we apply a Newton–Raphson iterative methodology to minimize the difference between predicted and observed velocities to calculate temperature as in Porter et al. [2019]. In our calculations, pressure is estimated using the crustal thickness model from Porter et al. [2016] and assuming a density of 2700 kg/m^3 for the crust. For calculating mantle densities, we follow the methodology of Goes et al. [2000], which accounts for the effects of pressure and temperature on upper mantle densities. Grain size is not well constrained within the mantle and may strongly influence the relationship between seismic velocities and temperatures, especially at elevated temperatures [*Jackson and Faul*, 2010; *McCarthy et al.*, 2011; e.g. *Dannberg et al.*, 2017]. As grain size may vary laterally and with depth within the upper mantle [e.g. *Karato and Wu*, 1993; *Behn et al.*, 2009], we assume a grain size of 1 mm in our estimates and show LAB estimates assuming grain size of 0.1 mm in the Supplemental Data.

In our seismic temperature calculations, we assume that all velocity variations in the mantle are associated with temperature, which does not account for the effects of composition, melts, fluids, etc. on shear velocities. The relative effects of these factors on seismic velocity are variable and debated [*Anderson and Sammis*, 1970; *Karato*, 1995; *van der Lee*, 2002; *Cammarano et al.*, 2003; *Dunn and Forsyth*, 2003; *Artemieva et al.*, 2004; *Kreutzmann et al.*, 2004; *Priestley and Mckenzie*, 2006; *Schutt and Lesher*, 2006; *Aizawa et al.*, 2007; *Schutt and Dueker*, 2008; *Karato*, 2010b; *Schutt and Lesher*, 2010; *Priestley and Mckenzie*, 2013; *Cammarano and Guerri*, 2017; *Cline et al.*, 2018]. While attributing all mantle seismic variations to temperature is a simplification of upper mantle conditions, this allows for a baseline

estimate of thermal conditions under the continent. For a more detailed discussion of these compositional assumptions and the methodology refer to Porter et al. [2019].

We use our seismically derived estimates of temperatures to calculate geotherms at every gridpoint within the shear velocity model. In order to estimate the thickness of the thermal lithosphere, we use the depth of the intersection of the 1300° C adiabat and seismically derived geotherms as a proxy for the location of the LAB (Figure 1). We also use these data to calculate the geothermal gradient in the upper mantle by measuring the vertical gradient of the estimated temperatures.

Basalt Thermobarometry

We calculate melt equilibrium pressure and temperatures using the major element thermobarometer described in Plank and Forsyth [2016]. Major oxide chemistries from basaltic rocks are downloaded from the EarthChem Portal (www.earthchem.org/portal) for all samples younger than 6 Ma within the western US and converted to molar percentages. The ratio of Fe^{3+} to Fe^{2+} is estimated assuming buffering of oxygen fugacity at the QFM buffer [*Kress and Carmichael*, 1991]. Whole rock compositions are converted to primary melt compositions by the sequential addition of olivine to obtain a melt in equilibration with Fo_{90}, as in *Lee et al.* [2009]. For our calculations, samples with less than 8% MgO, and/or 12% Al_2O_3, or those with unnormalized compositions of less than 97.5% by weight are deemed unlikely representative of near-primary mantle melts and were discarded. We estimate equilibrium P-T conditions assuming 1.5 wt % H_2O in the melt because water measurements are not available for most samples. The 1.5% value was chosen as a rough average based on the water contents observed by Plank and Forsyth [2016], which ranged from 1-3.2%.To account for the range of possible magmatic water contents, the error bars in Figures 3, and 4 show the range of temperatures

(horizontal) and pressures (vertical) that are calculated when water contents were varied between 0.5 wt % and 3 wt %. We compare our results to Plank and Forsyth [2016], who use vanadium to constrain oxygen fugacity and estimate Fe^{3+} to Fe^{2+} ratios. Resulting pressure-temperature estimate differences between our estimates and those of Plank and Forsyth [2016] are < 0.06 GPa and < 14º C when calculations were run for the same compositions assuming the same magmatic water contents.

Seismic Mantle Melting Estimates

In order to better understand the physical state of the upper mantle across the continent, we combine our seismic temperature estimates with experimental data that constrain solidi to map out where partial melt is present in the upper mantle across the contiguous US, assuming a peridotite upper mantle [*Katz et al.*, 2003]. The solidus was calculated for upper mantle depths assuming 75 ppm H_2O. We do not account for CO_2 in these melting estimates, which has a considerably smaller effect than H_2O and is negligible for melt equilibration pressures <2 GPa [*Plank and Forsyth*, 2016]. At temperatures above the solidus, the presence of partial melt is expected within the upper mantle, which would lower seismic velocities, and lead to an overestimation of seismically derived temperatures. Because of the uncertainty in this relationship, instead of estimating melt fractions based on temperature, we subtract solidus temperatures from our seismically derived temperatures estimates. This allows us to predict where partial melting is expected within the upper mantle.

The value of 75 ppm water was selected as a wet average for “damp” upper mantle. Previous geophysical estimates are consistent with 0-100 ppm water within the upper mantle outside of subduction zones [*Khan and Shankland*, 2010]. In actuality, hydration is likely variable both vertically and horizontally within the upper mantle [*Karato*, 2010a]. At a

continental scale, higher water contents are likely present in the western US than in the eastern and central parts of the country due to the recent history of subduction across the region [*Humphreys et al.*, 2003]. At a finer scale, hydration is likely variable regionally due to variations in geologic settings including lateral heterogeneity in slab dehydration [*Dixon et al.*, 2004], the extent of fluid introduction into the upper mantle during continental formation [*Selverstone et al.*, 1999], and post-formational processes such as cratonic rejuvenation [*Rudnick et al.*, 1998; *Carlson*, 2005; *Griffin et al.*, 2009; *Lee et al.*, 2011; *Eeken et al.*, 2018]. Compounding this uncertainty in the efficacy of hydration, mantle dehydration due to heating and related volcanism is likely inconsistent across the continent. The results reported here should help guide where expanded constraints on mantle hydration are imperative for better constraining the thermal and viscosity structure of the upper mantle.

RESULTS

Results of the seismic temperature calculations show large variations in the thermal regimes within the upper mantle across the continental US. As expected, cooler temperatures are observed throughout the uppermost mantle within the tectonically quiescent eastern and central US relative to tectonically active western US (Figures 1, 2, and 3). The hottest temperatures and thinnest lithosphere within the western US correspond to regions of recent extension and/or hypothesized mantle upwelling.

Melt thermobarometry estimates are primarily for generation of recently emplaced basalts in the Snake River Plain, the Basin and Range/Colorado Plateau margins, and the Cascade Arc (Figure 3). We show results from all samples though a few give erroneous results that result in pressure estimates less than that at the Moho (e.g. the low-P CP sample in Figure 3). Pressure-

160 temperature estimates from the Snake River Plain and Colorado Plateau generally exhibit
161 relatively high equilibrium temperatures and deeper depths than those within the Cascades, even
162 before the higher water contents likely present under the Cascades are considered (Figures 3 and
163 4). Our seismically derived thermal estimates generally agree well with the melt
164 thermobarometry results (Figures 3 and 4). Where seismic geotherms do not agree with
165 thermobarometry estimates, it is often in places where sharp lateral changes in upper mantle
166 temperature occur (e.g. the edges of the Snake River Plain). In the seismic model, these
167 boundaries may appear gradational due to smoothing. At pressures > 2 GPa, the Plank and
168 Forsyth [2016] estimates plot closer to the 1300° C adiabat, likely because of the higher water
169 contents in those samples (> 2 wt. % for many) than the fixed value used here. When we assume
170 greater degrees of hydration (indicated by the horizontal error bars in Figures 3 and 4) the
171 temperature estimates are relatively consistent between our estimates and Plank and Forsyth
172 [2016]. In comparing our seismic estimates of temperature to basalt equilibrium estimates, it is
173 apparent that volatiles are required to produce melts at depth > 2 GPa, as few seismically derived
174 geotherms show conditions hot enough to match PT estimates for basalts containing 1.5 wt %
175 water. This is consistent with hydration of the upper mantle beneath the Colorado Plateau and
176 parts of the western US due to the dehydration of a flat-slab during present beneath the region
177 during the late Cretaceous/Early Cenozoic.

178 In our seismic results, thinned thermal lithosphere (< 100 km thick) is observed across
179 much of the Basin and Range Province, beneath the Snake River Plain/Yellowstone hotspot
180 trace, and in the backarc of the Cascade Mountains in Washington and Oregon (Figures 1 and 2).
181 The thickest lithosphere (> 180 km thick) is observed in the central US where the cratonic core
182 of the continent is located. The shear model used to derive temperatures only has resolution

183 down to ~200 km depth; as such, estimates of ~200 km are likely a minimum thickness for
184 thermal lithosphere in cratonic regions and are not well-constrained. Intermediate lithospheric
185 thicknesses are observed along the eastern margin of the continent where rifting occurred during
186 the opening of the Atlantic Ocean in the Jurassic. A west-east cross section of temperature across
187 the continent highlights these variations in temperatures and depth to the thermal LAB (Figure
188 2). These results agree with body-wave tomography results which show a high-velocity keel
189 beneath the cratonic region of North America that extends down to ~200 km depth [*Schmandt*
190 *and Lin*, 2014], and with previous temperature estimates for the uppermost mantle [*Goes and van*
191 *der Lee, 2002; Schutt et al.*, 2018]. Thermal estimates also show slightly increased
192 temperatures/thinned thermal lithosphere along the eastern seaboard in the vicinity of New
193 England and western Virginia (Figure 1). These high temperature zones align with areas where
194 recent tectonism has been proposed [*van der Lee et al.*, 2008; *Mazza et al.*, 2014; *Schmandt and*
195 *Lin*, 2014; *Menke et al.*, 2016].

196 Zones of partial melting were mapped by identifying regions where seismically derived
197 geotherms exceed the predicted pressure-dependent solidus for peridotite with 75 ppm water.
198 Figure 3 shows the maximum difference between the seismically derived temperature estimates
199 and the peridotite solidus at all depths for gridpoints using the parameterization of Katz et al.
200 [2003]. Results show that partial melt is likely present within the mantle across much of the
201 western US, where thin lithosphere is observed, and absent within the eastern and central US
202 where the lithosphere is thicker.

203 Within the western US, the LAB may be defined by a zone of significant partial melting,
204 which would lower both mantle viscosity and, if enough partial melt were present, seismic
205 velocities. This sharp velocity gradient would result in a relatively sharp LAB conversion in

receiver functions. Basaltic volcanism in the western US is most commonly observed within the Basin and Range province where widespread extension, large-scale mantle upwelling, and small-scale convection have been proposed, and within the Snake River Plain where mantle upwelling associated with the Yellowstone hotspot is driving volcanism. In the eastern and central US, melts are predicted to be absent at the LAB for mantle containing 75 ppm water and the transition from lithosphere to asthenosphere may involve a gradual transition in viscosity.

A cross section of geothermal gradient highlights the varying temperature regimes within the upper mantle across the continental US (Figure 2). Higher gradients (> 2° C/km) are observed within the thermally defined (< 1300° C) lithospheric mantle than within areas mapped as asthenosphere (> 1300° C). These variations are consistent with conduction as the dominant mechanism of heat transfer in the lithosphere and advection or convection as the dominant mechanisms of heat transfer in the asthenosphere (Figure 2). In a few locations in the western US, low geothermal gradients are observed in regions where observed mantle temperatures are below 1300° C. Low gradients in these regions can be explained by uncertainty in the model and/or the presence of partial melt in these regions (Figure 2), which would likely allow for advective heat transfer. It is also possible that partial melting of these regions may lower the viscosity of the mantle enough for convective heat transfer to occur. In these cases, the 1300° C isotherm would likely be an inaccurate proxy for rheological lithospheric thickness.

DISCUSSION

Nature of the Lithosphere-Asthenosphere Boundary

In this work, we show that upper-mantle thermal conditions within much of the western US are near or above the solidus for partially hydrated peridotite (Figure 2), consistent with the

hypothesis that partial melt may play a role in controlling the thickness of mantle lithosphere in this region [*Hopper and Fischer*, 2018]. The presence or absence of partial melt in the upper mantle may influence how the rheological LAB, which separates viscous lithosphere from the lower viscosity asthenosphere [e.g. *Fischer et al.*, 2010], is observed seismically. In the western US, Sp receiver function work shows a laterally extensive high-amplitude negative conversion interpreted as the LAB, which can be explained by the presence of partial melt at this boundary and an abrupt boundary between lithosphere and asthenosphere [*Abt et al.*, 2010; *Hopper and Fischer*, 2018]. In the central cratonic US, mid-lithosphere seismic discontinues are observed in receiver functions, however, there is no conversion that can be clearly associated with the LAB. This lack of a clear boundary is consistent with a gradual transition from lithosphere to lower-viscosity asthenosphere in these regions [*Abt et al.*, 2010; *Hopper and Fischer*, 2018]. Within the eastern US, receiver function amplitudes are consistent with partial melt at the LAB [*Hopper and Fischer*, 2018], however, we do not observe temperatures high enough to result in melting without volatile addition (Figure 4).

Based on our seismically derived temperature estimates and the timing of tectonism, extensive upper mantle melting is expected only in areas with recent thermotectonic activity. This is highlighted in Figure 4 which shows geotherms taken from our model at gridpoints located at 1° latitude and longitude intervals. These geotherms are shaded using the thermotectonic age model of Porter et al. [2019], which is based on dating of surface volcanic rocks. Of these geotherms, the 75 ppm solidus is only exceeded by those with nearby young (< 10 Ma) volcanism. Figure 4 highlights the importance of thinned lithosphere in the occurrence of melting. In all but the hottest geotherms, melting with moderate hydration can only occur at relatively shallow depths (< ~100 km) within the mantle. Given this constraint, partial melt is

likely to define and yield a sharp LAB, observable in receiver functions, within regions of relatively thin and recently modified lithosphere or in areas carbonated and/or hydrated by extensive metasomatism.

Carbon dioxide-assisted melting is hypothesized as a mechanism for controlling the LAB by lowering the peridotite solidus in cratonic regions [*Tharimena et al.*, 2017]. The presence of carbon dioxide (in addition to water) can significantly lower the peridotite solidus [*Foley et al.*, 2009] and has been hypothesized as especially important for producing small-degree melting at depth within the mantle beneath mid-ocean ridges [*Dasgupta and Hirschmann*, 2006]. Our results are consistent with temperature exceeding the carbonated peridotite solidus at depths between 100-180 km in cratonic regions. However, this depth is shallower than our thermally derived LAB under the cratonic region of the US. Modeling work shows that, if the LAB is defined rheologically, the viscosity contrast at this boundary is between 3 and 10 orders of magnitude [*Doglioni et al.*, 2011; *Rolf et al.*, 2018]. To produce a velocity contrast of this magnitude between a solid and partially molten rock, a melt fraction, φ, > 0.2 is required [*Kohlstedt and Hansen*, 2015]. Such a melt fraction, even if arising from magma pooling, would require widespread carbonization and/or hydration of the upper mantle to produce an extensive region with this degree of melting. Because of this, we prefer a thermal rather than melt-related explanation for the LAB under the cratonic US that results in a gradational boundary.

CONCLUSIONS

Results from this work highlight the varied thermal states of the upper mantle across the continental US and shed insight into the nature of the lithosphere-asthenosphere boundary within the region. In our measurements, we observe hotter temperatures and zones of extensive melting

in the western US that are absent in the central and eastern US. These zones of mapped melts align well with recently emplaced basalts at the surface. Melt within the tectonically active western US likely defines the LAB while this is less likely in cratons where melts would only form in zones of concentrated metasomatism.

ACKNOWLEDGMENTS

This work was funded by NSF Award EAR-1829520. Seismic data were collected as part of the EarthScope experiment and downloaded from the IRIS DMC.

DATA AVAILABILITY STATEMENT

Data from the TA network were made freely available as part of the EarthScope USArray facility, operated by Incorporated Research Institutions for Seismology (IRIS) and supported by the National Science Foundation, under Cooperative Agreements EAR-1261681. No new data were collected as part of this work, the seismic data used can be accessed at: https://ds.iris.edu/ds/nodes/dmc/. The geochemical data are available at: www.earthchem.org/portal.

FIGURE CAPTIONS

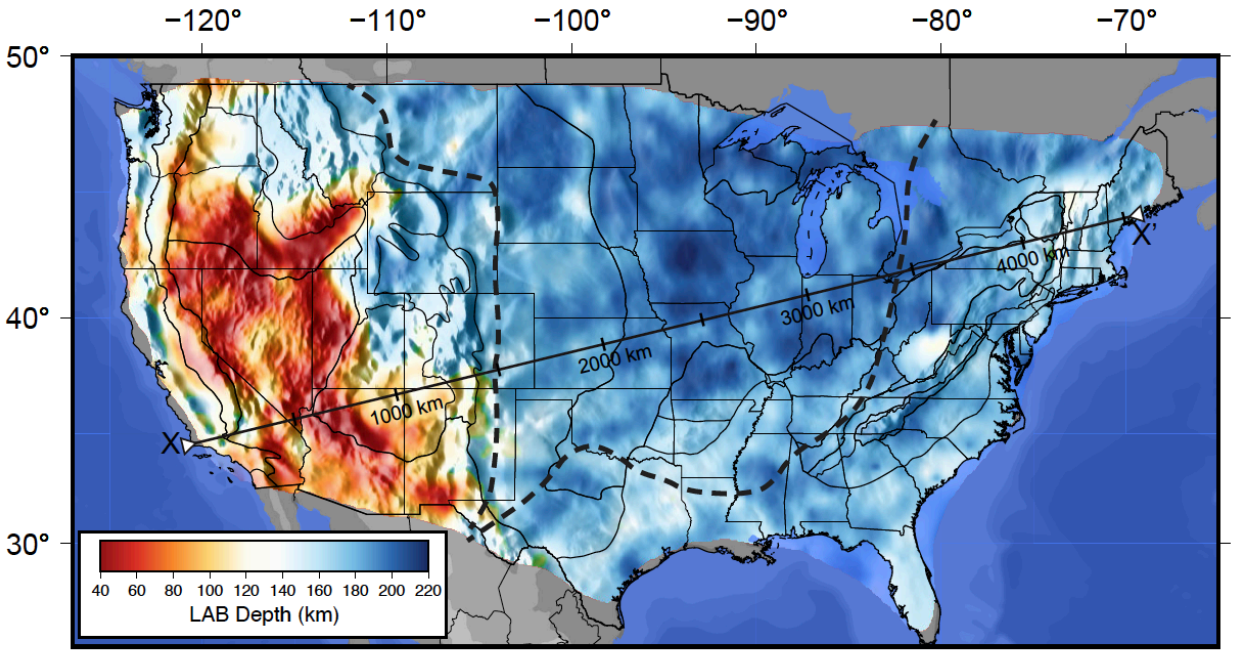

Figure 1. Map of depth to the 1300° C adiabat, which is interpreted as the base of the thermal lithosphere. Bold lines are physiographic provinces modified from Fenneman [1917]. Thick dashed line denotes the Grenville Front and eastern limit of Cordilleran strain [*DeCelles*, 2004; *Whitmeyer and Karlstrom*, 2007]. Line X-X' shows the location of the cross section in Figure 2. Hill shade shows topography.

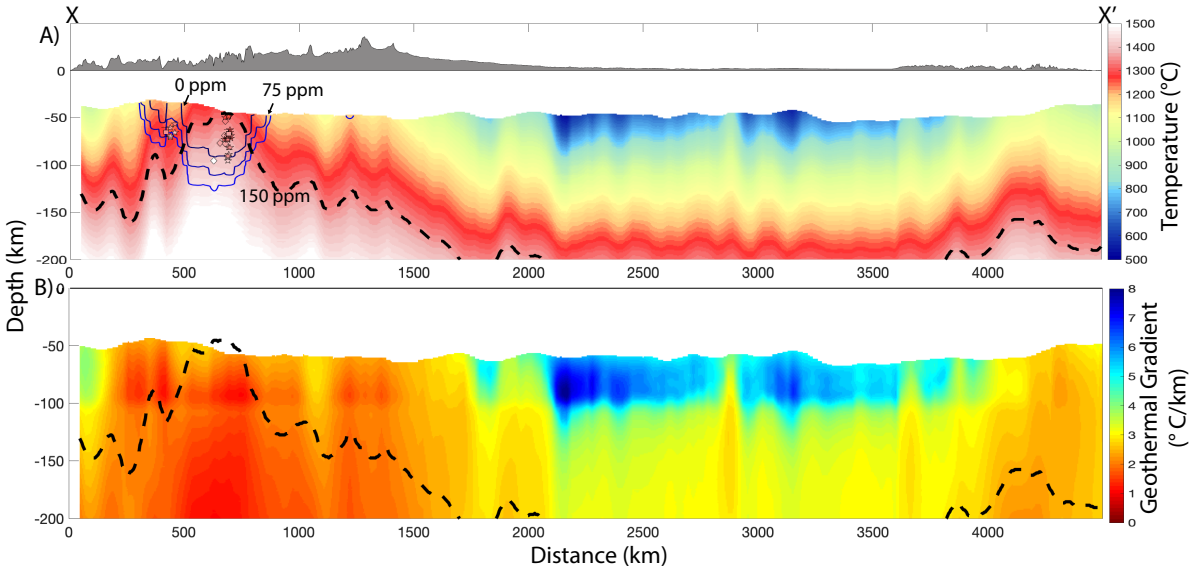

299

300 Figure 2. Thermal profiles along line X-X'. Panel A shows seismically derived upper mantle
301 temperature estimates. The dashed black line is where the modeled temperatures reach the 1300°
302 C adiabat, which we interpret as the thermal LAB. The thin blue lines are the estimated solidi
303 assuming anhydrous conditions (dark blue), 75 ppm water (medium blue), and 150 ppm water
304 (light blue). Melt is expected in the regions above these curves. Diamond are basalt melt
305 equilibrium P-T conditions from this study. Fill colors indicate temperature estimates. Stars are
306 P-T conditions from Plank and Forsyth [2016] and squares are from Klöcking [2018]. Panel B
307 shows smoothed geothermal gradient for cross section X-X'. Higher geothermal gradients are
308 observed in cratonic areas with thick lithosphere relative to areas of thinned lithosphere. Dashed
309 line is the thermal LAB.

310

311

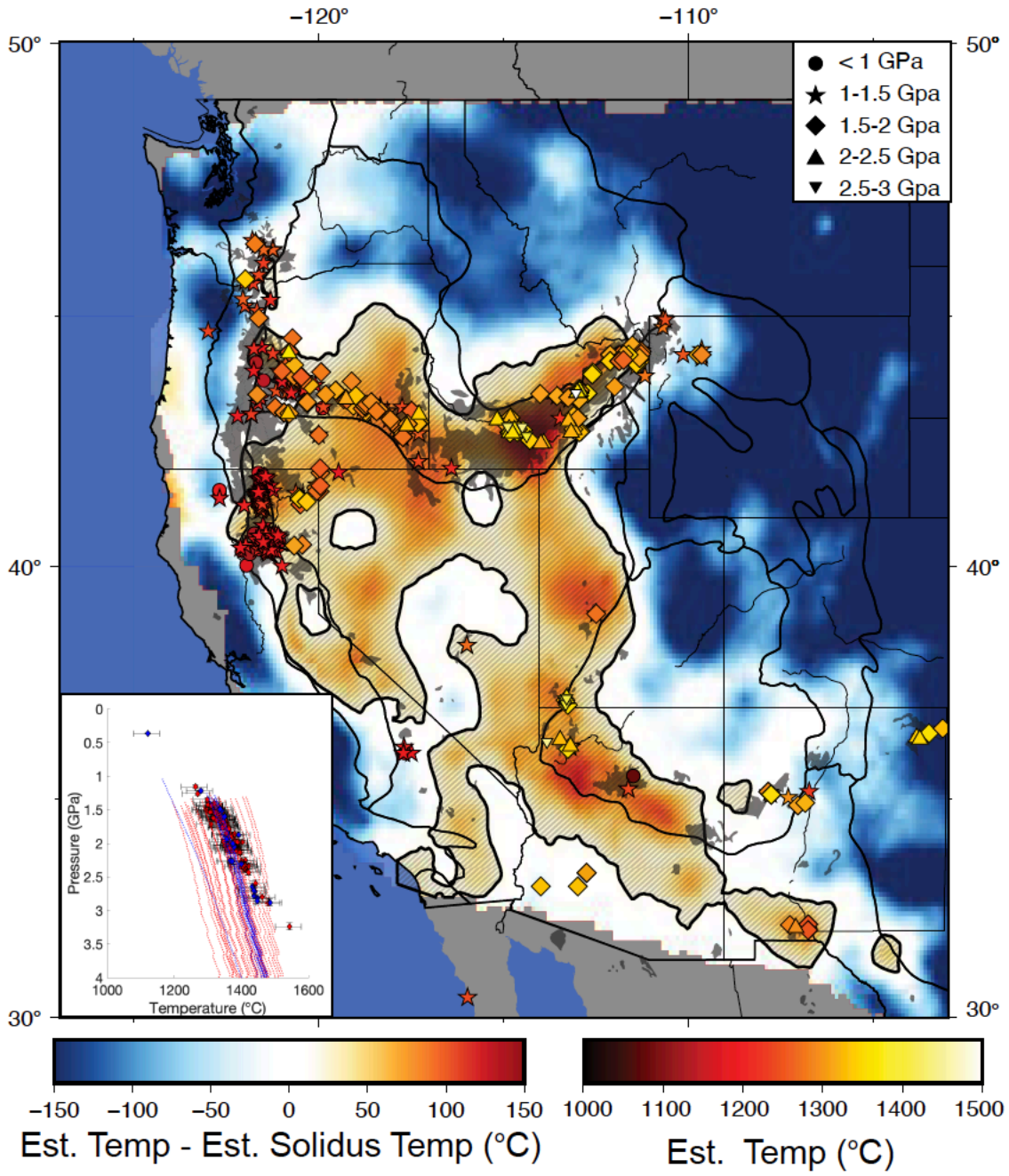

312

313 Figure 3. Map showing maximum temperature difference between seismically estimated mantle

314 temperatures (T_{est}) and the temperature of the solidus (T_{sol}) for partially hydrated (75 ppm)

315 peridotite at all depths for each gridpoint (i.e. max($T_{est}(d)$ - $T_{sol}(d)$) where d is every depth in the

316 model). Melt is expected in areas where positive values are observed. Plotted symbols indicate

the location, temperature and pressure of melt thermobarometry data. Black regions are mapped Pliocene and younger volcanic units from the Decade of North American Geology: Geologic Map of North America [*Reed et al.*, 2005]. Physiographic provinces modified from Fenneman [1917]. Inset shows the melt equilibrium estimates (diamonds) and the closest seismically derived geotherm (dotted lines) from the Colorado Plateau (blue) and Snake River Plain (red). The spread in Snake River Plain seismic geotherms is due to the sharp boundaries of the province.

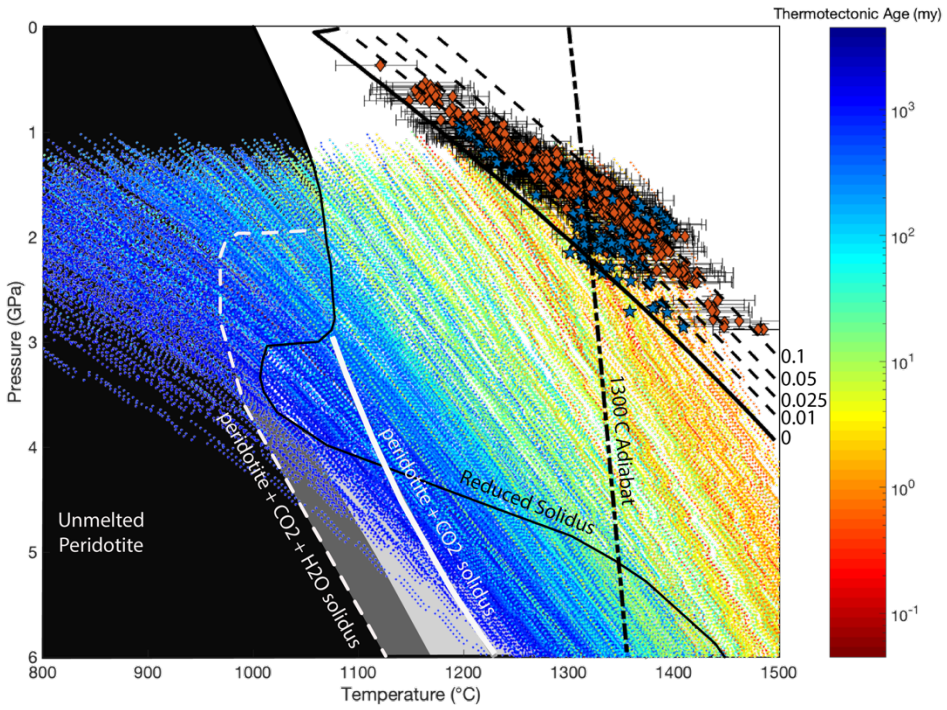

Figure 4. Pressure-temperature plots of seismic and basalt melt equilibrium data. Dotted lines are seismically derived geotherms for the continental US taken at 1° intervals. Geotherms colors are based on thermotectonic age for their location using the model of Porter et al. [2019]. Orange diamond are basalt melt equilibrium P-T conditions from this study. Error bars show the effects of varying water contents between 0.5 wt % and 3 wt % on temperature (horizontal) and pressure (vertical) for each sample. Blue stars are P-T conditions from Plank and Forsyth [2016]. Solid

black line is the solidus and labeled dashed contour lines are melt fractions based on Katz et al. [2003] for 75 ppm water in the upper mantle. The sub-vertical dashed black line is the 1300° C adiabat. Background shading and additional lines are CO_2 solidi modified from Foley et al. [2009].

REFERENCES CITED

Abt, D. L., K. M. Fischer, S. W. French, H. A. Ford, H. Yuan, and B. Romanowicz (2010), North American lithospheric discontinuity structure imaged by Psand Spreceiver functions, *J Geophys Res-Solid*, *115*(B9), B09301, doi:10.1029/2009JB006914.

Aizawa, Y., A. Barnhoorn, U. H. Faul, J. D. Fitz Gerald, I. Jackson, and I. Kovacs (2007), Seismic Properties of Anita Bay Dunite: an Exploratory Study of the Influence of Water, *J Petrol*, *49*(4), 841–855, doi:10.1093/petrology/egn007.

Anderson, D. L., and C. Sammis (1970), Partial melting in the upper mantle, *PEPI*, *3*, 41–50, doi:10.1016/0031-9201(70)90042-7.

Artemieva, I. M., M. Billien, J.-J. Lévêque, and W. D. Mooney (2004), Shear wave velocity, seismic attenuation, and thermal structure of the continental upper mantle, *GeoJI*, *157*(2), 607–628, doi:10.1111/j.1365-246X.2004.02195.x.

Behn, M. D., G. Hirth, and J. R. Elsenbeck II (2009), Implications of grain size evolution on the seismic structure of the oceanic upper mantle, *E&PSL*, *282*(1-4), 178–189, doi:10.1016/j.epsl.2009.03.014.

Cammarano, F., and M. Guerri (2017), Global thermal models of the lithosphere, *GeoJI*, *210*(1), 56–72, doi:10.1093/gji/ggx144.

Cammarano, F., S. Goes, P. Vacher, and D. Giardini (2003), Inferring upper-mantle temperatures from seismic velocities, *PEPI*, *138*(3-4), 197–222, doi:10.1016/S0031-9201(03)00156-0.

Carlson, R. W. (2005), Physical, chemical, and chronological characteristics of continental mantle, *Rev Geophys*, *43*(1), 1–24, doi:10.1029/2004RG000156.

Cline, C. J., U. H. Faul, E. C. David, A. J. Berry, and I. Jackson (2018), Redox-influenced seismic properties of upper- mantle olivine, *Nature*, *555*(7696), 355–358, doi:10.1038/nature25764.

Crotwell, H. P., and T. J. Owens (2005), Automated receiver function processing, *Seismological Research Letters*, *76*(6), 702–709.

Dannberg, J., Z. Eilon, U. Faul, R. Gassmöller, P. Moulik, and R. Myhill (2017), The importance of grain size to mantle dynamics and seismological observations, *Geochemistry, Geophysics, Geosystems*, *18*(8), 3034–3061, doi:10.1002/2017GC006944.

Dasgupta, R., and M. M. Hirschmann (2006), Melting in the Earth's deep upper mantle caused by carbon dioxide, *Nature*, *440*(7084), 659–662, doi:10.1038/nature04612.

DeCelles, P. G. (2004), Late Jurassic to Eocene evolution of the Cordilleran thrust belt and foreland basin system, western USA, *AmJS*, *304*(2), 105.

Dixon, J. E., T. H. Dixon, D. R. Bell, and R. Malservisi (2004), Lateral variation in upper mantle viscosity: role of water, *E&PSL*, *222*(2), 451–467, doi:10.1016/j.epsl.2004.03.022.

Doglioni, C., A. Ismail-Zadeh, G. Panza, and F. Riguzzi (2011), Lithosphere–asthenosphere viscosity contrast and decoupling, *PEPI*, *189*(1-2), 1–8, doi:10.1016/j.pepi.2011.09.006.

Dunn, R. A., and D. W. Forsyth (2003), Imaging the transition between the region of mantle melt generation and the crustal magma chamber beneath the southern East Pacific Rise with short-period Love waves, *JGR*, *108*(B7), 641, doi:10.1029/2002JB002217.

Eeken, T., S. Goes, H. A. Pedersen, N. A. E. A. Planetary, 2018 (2018), Seismic evidence for depth-dependent metasomatism in cratons, *EPSL*, *491*, 148–159, doi:10.1016/j.epsl.2018.03.018.

Faul, U., and I. Jackson (2005), The seismological signature of temperature and grain size variations in the upper mantle, *E&PSL*, *234*(1-2), 119–134, doi:10.1016/j.epsl.2005.02.008.

Fenneman, N. M. (1917), Physiographic divisions of the United States, *Proceedings of the National Academy of Science of the United States of America*, *1*(3), 17–22, doi:10.1073/pnas.3.1.17.

Fischer, K. M., H. A. Ford, D. L. Abt, and C. A. Rychert (2010), The lithosphere-asthenosphere boundary, *Annu. Rev. Earth Planet. Sci.*, *38*(1), 551–575, doi:10.1146/annurev-earth-040809-152438.

Foley, S. F., G. M. Yaxley, A. Rosenthal, S. Buhre, E. S. Kiseeva, R. P. Rapp, and D. E. Jacob (2009), The composition of near-solidus melts of peridotite in the presence of CO2 and H2O between 40 and 60 kbar, *Litho*, *112*(S1), 274–283, doi:10.1016/j.lithos.2009.03.020.

Goes, S., R. Govers, and P. Vacher (2000), Shallow mantle temperatures under Europe from P and Swave tomography, *J Geophys Res-Solid*, *105*(B5), 11153–18, doi:10.1029/1999JB900300.

Goes, S. and van der Lee, S., (2002), Thermal structure of the North American uppermost mantle inferred from seismic tomography. *Journal of Geophysical Research: Solid Earth*, *107*(B3).

Griffin, W. L., S. Y. O'Reilly, J. C. Afonso, and G. C. Begg (2009), The Composition and Evolution of Lithospheric Mantle: a Re-evaluation and its Tectonic Implications, *J Petrol*.

Herrmann, R. B., and C. J. Ammon (2002), Computer Programs in Seismology–Surface Waves, Receiver Functions and Crustal Structure, *St. Louis University*.

Hopper, E., and K. M. Fischer (2018), The Changing Face of the Lithosphere-Asthenosphere Boundary: Imaging Continental Scale Patterns in Upper Mantle Structure Across the Contiguous U.S. With Sp Converted Waves, *Geochem. Geophys. Geosyst.*, *19*(8), 2593–2614, doi:10.1029/2018GC007476.

Humphreys, E., E. Hessler, K. Dueker, G. L. Farmer, E. Erslev, and T. Atwater (2003), How Laramide-age hydration of North American lithosphere by the Farallon slab controlled subsequent activity in the western United States, *International Geology Review*, *45*(7), 575–595.

Isaak, D. G. (1992), High-temperature elasticity of iron-bearing olivines, *JGR*, *97*(B2), 1871–1885.

Jackson, I., and U. H. Faul (2010), Grainsize-sensitive viscoelastic relaxation in olivine: Towards a robust laboratory-based model for seismological application, *PEPI*, *183*(1-2), 151–163, doi:10.1016/j.pepi.2010.09.005.

Jackson, J., D. Mckenzie, K. Priestley, and B. Emmerson (2008), New views on the structure and rheology of the lithosphere,, *165*, 453–465.

Jordan, T. H. (1975), The continental tectosphere, *Rev Geophys*, *13*(3), 1–12, doi:10.1029/RG013i003p00001.

Karato, S. (1995), Effects of Water on Seismic-Wave Velocities in the Upper-Mantle, *Proceedings of the Japan Academy Series B-Physical and Biological Sciences*, *71*(2), 61–66.

Karato, S. I. (2010a), Mapping water content in the upper mantle, in *Volcanism and Subduction: The Kamchatka Region*, vol. 138, pp. 135–152, American Geophysical Union, Washington, D. C.

Karato, S. I. (2010b), Rheology of the deep upper mantle and its implications for the preservation of the continental roots: A review, *Tectonophysics*, *481*(1-4), 82–98, doi:10.1016/j.tecto.2009.04.011.

Karato, S. I., and P. Wu (1993), Rheology of the Upper Mantle: A Synthesis, *Sci*, *260*(5109), 771–778.

Katz, R. F., Geochemistry, M. S., Katz, R. F., 2003, M. Spiegelman, M. Spiegelman, and C. H. Langmuir (2003), A new parameterization of hydrous mantle melting, *Geochem Geophy Geosy*, *4*, 19, doi:10.1029/2002GC000433.

Khan, A., and T. J. Shankland (2010), A geophysical perspective on mantle water content and melting: Inverting electromagnetic sounding data using laboratory-based electrical conductivity profiles, *E&PSL*, *317-318*, 1–17, doi:10.1016/j.epsl.2011.11.031.

Klöcking, M., N. J. White, J. Maclennan, D. Mckenzie, and J. G. Fitton (2018), Quantitative Relationships Between Basalt Geochemistry, Shear Wave Velocity, and Asthenospheric Temperature Beneath Western North America, *Geochem. Geophys. Geosyst.*, *19*(9), 3376–3404, doi:10.1029/2018GC007559.

Kohlstedt, D. L., and L. N. Hansen (2015), Constitutive Equations, Rheological Behavior, and Viscosity of Rocks, in *Constitutive equations, rheological behavior, and viscosity of rocks*, pp. 441–472, Elsevier.

Kress, V. C., and I. S. Carmichael (1991), The compressibility of silicate liquids containing Fe2O3 and the effect of composition, temperature, oxygen fugacity and pressure on their redox states, *Contrib Mineral Petr*, *108*(1-2), 82–92.

Kreutzmann, A., H. Schmeling, A. Junge, T. Ruedas, G. Marquart, and I. T. Bjarnason (2004), Temperature and melting of a ridge-centred plume with application to Iceland. Part II: Predictions for electromagnetic and seismic observables, *GeoJI*, *159*(3), 1097–1111, doi:10.1111/j.1365-246X.2004.02397.x.

Laske, G., and G. Masters (1997), A global digital map of sediment thickness, *Eos Trans. AGU*, *78*(F483).

Lee, C.-T. A., P. Luffi, and E. J. Chin (2011), Building and Destroying Continental Mantle, *Annu. Rev. Earth Planet. Sci.*, *39*(1), 59–90, doi:10.1146/annurev-earth-040610-133505.

Lee, C.-T. A., P. Luffi, T. Plank, H. Dalton, and W. P. Leeman (2009), Constraints on the depths and temperatures of basaltic magma generation on Earth and other terrestrial planets using new thermobarometers for mafic magmas, *E&PSL*, *279*(1-2), 20–33, doi:10.1016/j.epsl.2008.12.020.

Liu, Y., and W. E. Holt (2015), Wave gradiometry and its link with Helmholtz equation solutions applied to USArray in the eastern US, *J. Geophys. Res. Solid Earth*, doi:10.1002/(ISSN)2169-9356.

Mazza, S. E., E. Gazel, E. A. Johnson, M. J. Kunk, R. McAleer, J. A. Spotila, M. Bizimis, and D. S. Coleman (2014), Volcanoes of the passive margin: The youngest magmatic event in eastern North America, *Geol*, *42*(6), 483–486, doi:10.1130/G35407.1.

McCarthy, C., Y. Takei, and T. Hiraga (2011), Experimental study of attenuation and dispersion over a broad frequency range: 2. The universal scaling of polycrystalline materials, *JGR*, *116*(B9), 3893, doi:10.1029/2011JB008384.

Menke, W., P. Skryzalin, V. Levin, and T. Harper (2016), The Northern Appalachian Anomaly: A modern asthenospheric upwelling, *GRL*, *43*(19), 10,173–10,179, doi:10.1002/2016GL070918.

Plank, T., and D. W. Forsyth (2016), Thermal structure and melting conditions in the mantle beneath the Basin and Range province from seismology and petrology, *Geochem. Geophys. Geosyst.*, *17*(4), 1312–1338, doi:10.1002/2015GC006205.

Porter, R. C., S. van der Lee, and S. J. Whitmeyer (2019), Synthesizing EarthScope data to constrain the thermal evolution of the continental U.S. lithosphere, *Geosphere*, *15*(6), 1722–1737, doi:10.1130/GES02000.1.

Porter, R., Y. Liu, Y. Liu, W. E. Holt, and W. E. Holt (2016), Lithospheric records of orogeny within the continental US, *GeoRL*, *43*(1), 144–153, doi:10.1002/2015GL066950.

Priestley, K., and D. Mckenzie (2006), The thermal structure of the lithosphere from shear wave velocities, *E&PSL*, *244*(1-2), 285–301.

Priestley, K., and D. Mckenzie (2013), The relationship between shear wave velocity, temperature, attenuation and viscosity in the shallow part of the mantle, *E&PSL*, *381*, 78–91, doi:10.1016/j.epsl.2013.08.022.

Reed, J. C., B. E. Tucholke, and J. O. Wheeler (2005), Decade of North American Geology: Geologic Map of North America: Perspectives and Explanation,

Rolf, T., F. A. Capitanio, and P. J. Tackley (2018), Constraints on mantle viscosity structure from continental drift histories in spherical mantle convection models, *Tectonophysics*, *746*(C), 339–351, doi:10.1016/j.tecto.2017.04.031.

Rudnick, R. L., W. F. McDonough, and R. J. O'Connell (1998), Thermal structure, thickness and composition of continental lithosphere, *Chemical Geology*, *145*(3-4), 395–411, doi:10.1016/S0009-2541(97)00151-4.

Schmandt, B., and F.-C. Lin (2014), P and S wave tomography of the mantle beneath the United States, *GeoRL*, *41*, 1–8, doi:10.1002/(ISSN)1944-8007.

Schutt, D. L., A. R. Lowry, and J. S. Buehler (2018), Moho temperature and mobility of lower crust in the western United States, *Geol*, 1–4, doi:10.1130/G39507.1.

Schutt, D. L., and C. E. Lesher (2006), Effects of melt depletion on the density and seismic velocity of garnet and spinel lherzolite, *JGR*, *111*(B5), B05401, doi:10.1029/2003JB002950.

Schutt, D. L., and C. E. Lesher (2010), Compositional trends among Kaapvaal Craton garnet peridotite xenoliths and their effects on seismic velocity and density, *E&PSL*, *300*(3-4), 367–373, doi:10.1016/j.epsl.2010.10.018.

Schutt, D. L., and K. Dueker (2008), Temperature of the plume layer beneath the Yellowstone hotspot, *Geol*, *36*(8), 623–4, doi:10.1130/G24809A.1.

Selverstone, J., A. Pun, and K. C. Condie (1999), Xenolithic evidence for Proterozoic crustal evolution beneath the Colorado Plateau, *Geol Soc Am Bull*, *111*(4), 590–606, doi:10.1130/0016-7606(1999)111<0590:XEFPCE>2.3.CO;2.

Tharimena, S., C. Rychert, and N. Harmon (2017), A unified continental thickness from seismology and diamonds suggests a melt-defined plate, *Sci*, *357*(6351), 580–583.

van der Lee, S. (2002), High-resolution estimates of lithospheric thickness from Missouri to Massachusetts, USA, *E&PSL*, *203*(1), 15–23.

van der Lee, S., K. Regenauer-Lieb, and D. A. Yuen (2008), The role of water in connecting past and future episodes of subduction, *E&PSL*, *273*(1-2), 15–27, doi:10.1016/j.epsl.2008.04.041.

Whitmeyer, S. J., and K. E. Karlstrom (2007), Tectonic model for the Proterozoic growth of North America, *Geosphere*, *3*(4), 220.

Yuan, H., and B. Romanowicz (2010), Lithospheric layering in the North American craton, *Nature*, *466*(7310), 1063–1068, doi:10.1038/nature09332.